Cadmium-free silica-encapsulated molecularly imprinted AuZnCeSeS quantum dots nanocomposite as an ultrasensitive fluorescence nanosensor for methamphetamine detection

Adegoke, Oluwasesan; Nsuamani, M. Laura; Nic Daeid, Niamh

Published in:
Materials Science in Semiconductor Processing

DOI:
10.1016/j.mssp.2023.107387

Publication date:
2023

Materials Science in Semiconductor Processing 159 (2023) 107387

Contents lists available at ScienceDirect

Materials Science in Semiconductor Processing

journal homepage: www.elsevier.com/locate/mssp

Cadmium-free silica-encapsulated molecularly imprinted AuZnCeSeS quantum dots nanocomposite as an ultrasensitive fluorescence nanosensor for methamphetamine detection

Oluwasesan Adegoke *, M. Laura Nsuamani, Niamh Nic Daeid

Leverhulme Research Centre for Forensic Science, University of Dundee, Dundee, DD1 4HN, UK

A B S T R A C T

One of the major challenges facing forensic drug analysis is the difficulty in detecting ultralow concentration of illicit drugs in biological matrices without the need for an extraction or a pre-treatment step. This work report on the development of a novel AuZnCeSeS quantum dots (QDs)-molecular imprinted polymer (MIP) nanocomposite fluorescent probe for methamphetamine (METH) recognition. Silica-coated AuZnCeSeS QDs were synthesized and characterized using spectrophotometric, spectroscopic and electron microscopy techniques. Via a free radical polymerization reaction, a thin layer of MIP shell with METH as the template was coated around the QDs surface leading to the formation of a QDs-MIP nanocomposite probe. The MIP coating passivated the QDs surface leading to radiative fluorescence enhancement of the bound QDs. Under optimum reaction conditions, METH was selectively and quantitatively detected via a fluorescence quenching reaction process. The unique selectivity of the nanoprobe for METH recognition showed clearly that METH was able to precisely re-bind to the MIP surface with size and shape reorganization. While the MIP shell functioned to provide the required selectivity, the AuZnCeSeS QDs functioned to fluorescently report the surface binding interaction. The use of a AuZnCeSeS QDs-non-imprinted polymer as probe to detect METH resulted in poor sensitivity and selectivity; hence, demonstrating the suitability of the AuZnCeSeS QDs-MIP nanoprobe to accurately detect METH. METH was detected within a wide concentration range from 0.05 to 50,000 nM with a detection limit of ~0.02 nM (0.0036 ng/mL). The developed AuZnCeSeS QDs-MIP nanoprobe was efficiently used to detect METH in untreated urine sample with recovery efficiency from ~100 to 110%.

1. Introduction

Methamphetamine (METH) is a well-known potent sympathomimetic amphetamine type stimulant drug that functions by inducing biogenic amine release in the brain, specifically dopamine and norepinephrine, leading to heightened feeling of alertness, exhilaration, euphoria and well-being, as well as increased sexual arousal and diminished appetite [1,2]. Psychotic behaviour and hallucination caused by serotonin and dopamine release in the mid-brain are abnormalities observed when high dose of METH is taken [3]. METH has also been used to treat alcoholism and obesity, however, when used, it can cause psychological and physiological effects such as increased blood pressure, heart rate which affects mood, attention and body temperature. It has also been reported to be one of the widely abused drugs in the world [4,5]. Rapid and accurate (both sensitive and selective) detection of METH is important as it will assist law enforcement in combating and preventing illicit drug production distribution and trafficking. It is also important from a medical perspective as it would allow medical personnel to make proper judgement in administering swift medication for overdosed drug users.

Methods which have been used to detect METH includes chromatographic techniques such as high-performance liquid chromatography (HPLC), gas chromatography (GC) and LC-mass spectrometry (LC-MS and GC-MS) [6–9]. Electrochemiluminescence [10], solid phase microextraction capillary electrophoresis [11], colorimetry [12], ion mobility spectrometry [13], surface-enhanced Raman spectroscopy [14], electrochemistry [15], fibre optic particle plasmon resonance [16] and fluorescence spectrophotometry [17], are other techniques that have been used for METH detection. Chromatographic techniques which are the most commonly used method for confirmatory testing of illicit drugs, require time consuming complex sample preparation and highly skilled personnel for operation and are expensive to operate. Analytical techniques with the potential to detect METH in biological matrices without extraction or pre-treatment is also a huge challenge for forensic drug analysis. There is therefore a strong demand for the development of rapid, portable, and accurate sensor systems for the quantitative detection of METH as increased concern over its usage grows in Europe [4,18]. This work addresses this challenge through the development of a fluorescence nanosensor for METH analysis.

In order to rapidly, selectively and sensitively detect ultralow

* Corresponding author. Leverhulme Research Centre for Forensic Science, School of Science & Engineering, University of Dundee, Dundee, DD1 4GH, UK.
E-mail address: o.adegoke@dundee.ac.uk (O. Adegoke).

https://doi.org/10.1016/j.mssp.2023.107387
Received 2 January 2023; Received in revised form 2 February 2023; Accepted 6 February 2023
Available online 11 February 2023

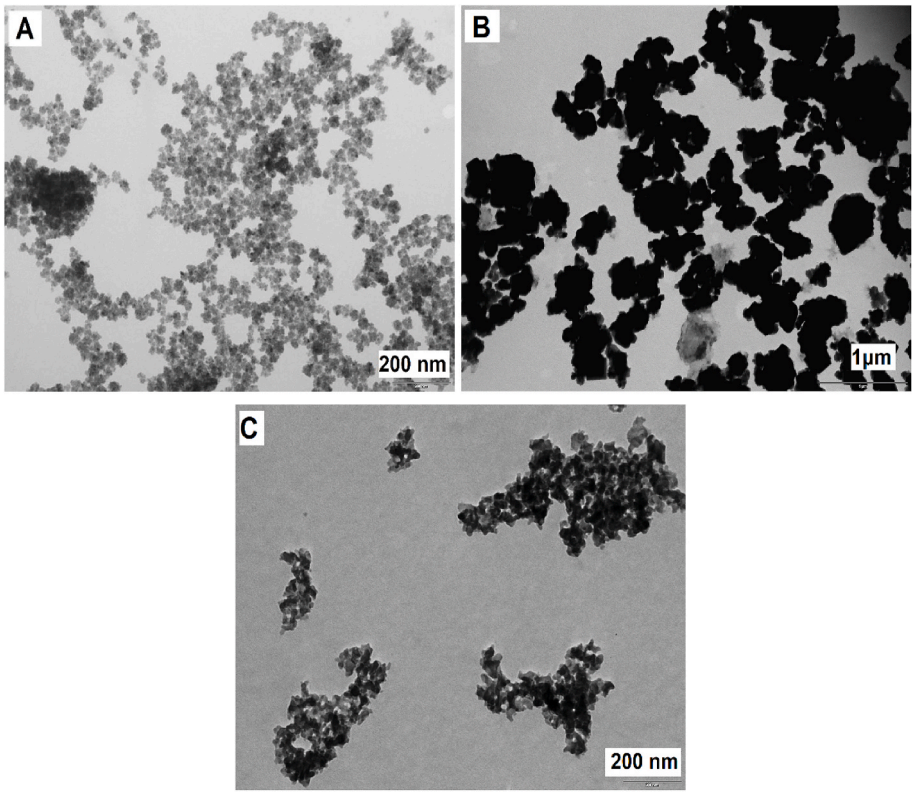

Fig. 1. TEM images of MPA-capped AuZnCeSeS QDs, SiO_2-AuZnCeSeS QDs and the AuZnCeSeS QDs-MIP nanocomposite.

concentration of an analyte, affinity-based fluorescence nanosensors with embedded nanofluorophores (as fluorescence reporters) and receptors (as recognition binding elements), have found wide applications in several fields, including the detection of environmental pollutants [19], viruses [20,21], disease biomarkers [22], drugs [23], and toxic metal ions [24], etc. Specifically, the sensitivity of affinity-based fluorescence nanoassays is strongly dependent on the functional properties of the nanomaterials. Over the past three decades, semiconductor quantum dot (QD) nanocrystals have attracted significant interest as excellent nanofluorophores due to their size-tunable broad absorption and narrow emission spectra, higher photostability against photodegradation, increased brightness, and higher surface area-to-volume ratio [25,26]. QDs have generally been used to develop affinity-based fluorescent probes with receptor recognition elements such as antibodies [27], DNA aptamers [28] and molecularly imprinted polymers (MIP) [29]. Antibodies, though widely known, are limited to mild conditions because denaturation of protein occurs under extreme pH and temperature conditions. In addition, they are costly and time consuming to produce and due to the challenges of immobilization on transducer surfaces, immunosensors are highly prone to false positive and false negative results [30]. DNA aptamers on the other hand, are more stable than antibodies; however, they are costly to produce and are extremely limited in availability as only limited research groups across the world have the expertise to develop them via computational biology. Hence, alternative synthetic receptors such as MIPs, which are universal, cheap to produce, readily available, stable and highly selective to the target of interest, are of high interest in mainstream affinity-based sensor research.

MIP was first developed by Wuff and Sarhan in 1972 [31] and since then, a plethora of studies have demonstrated the use of MIPs as artificial synthetic receptors for chemical sensing [32,33], as adsorbent in analytical separation [34] and as drug delivery agents in *in vivo* studies [35]. The general concept of a MIP involves prepolymer polymerization in the presence of the target analyte called the template. Bonds which are formed between the template and polymer during the curing process can be thought to emanate from the self-assembling of the embedded monomers. Positive charges within the prepolymer complex will generally align towards the negative charges of the template molecule. This phenomenon aligns with several noncovalent interactions such as hydrogen bonding, π-π bonding and hydrophobic and ionic interactions. During the polymerization process, fixed interaction regions are created from the cross-linked oligomers. The created cavities will then reproduce the shape and size of the template even after the template has been removed. In general, noncovalent interaction between the created cavity and the template molecule is highly favoured as the template can be removed much easily [36]. To date, there are several reported QDs-MIP nanocomposite detection systems where the QDs functioned as a core platform to transduce the fluorescence signal based on surface binding interactions. The MIP on the other hand, functioned as a shell layer to generate the required assay specificity [29,37–39]. To the best of our knowledge, there is only one report on the use of graphene QDs-MIP nanocomposite for METH detection [40] and no work on the use of semiconductor QDs-MIP nanocomposite for METH detection has been reported.

In this work, we report on the development of a novel cadmium-free semiconductor QDs-MIP nanocomposite detection system for METH. Alloyed AuZnCeSeS QDs were synthesized via the hot pyrolysis of metal precursors, organophosphorus surfactants and organic capping ligands and surface-capped with 3-mercaptopropionic acid (MPA) to render the QDs hydrophilic, biocompatible and stable. MPA-capped AuZnCeSeS QDs was then subsequently coated with amine (NH_2)-silica and a free radical polymerization reaction was carried out to overcoat the MIP around the QDs with METH as the template. The developed AuZnCeSeS QDs-MIP nanocomposite fluorescent probe was successfully used to detect METH rapidly and selectively with ultrahigh sensitivity that has never been reported before in the literature. Additionally, the detection of METH in biological matrices using the developed AuZnCeSeS QDs-MIP nanoprobe was attempted in this work.

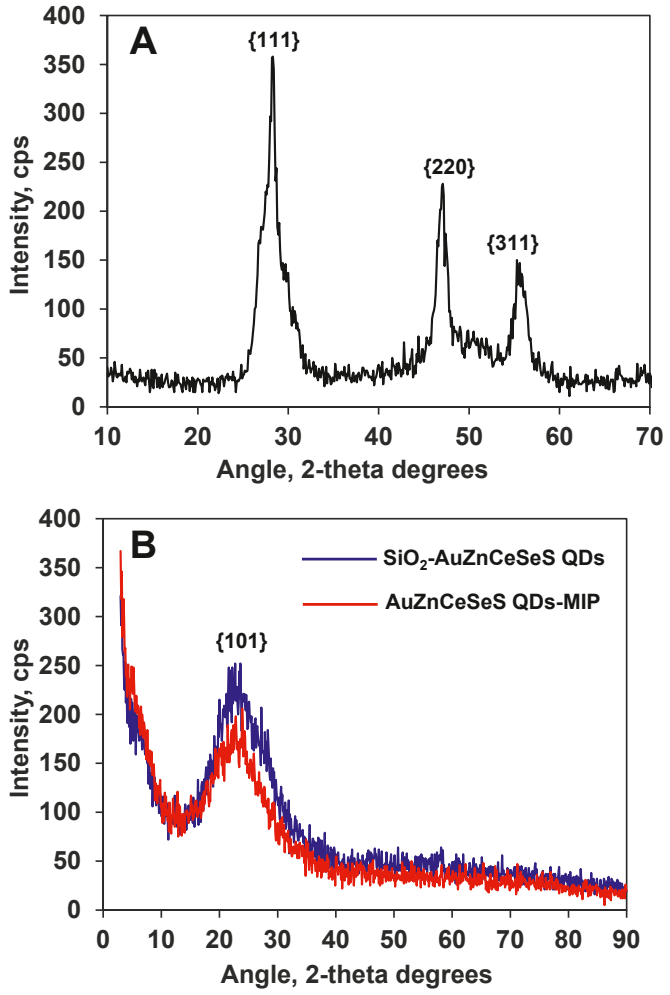

Fig. 2. XRD pattern for MPA-AuZnCeSeS QDs (A), SiO_2-AuZnCeSeS QDs and the AuZnCeSeS QDs-MIP nanocomposite.

2. Experimental

2.1. Chemicals

Acrylamide, ethylene glycol dimethacrylate (EGDMA), paracetamol (PARA), methamphetamine hydrochloride (METH), cocaine hydrochloride, 3-aminopropyl)triethoxysilane, amphetamine hydrochloride (AMP), oleylamine, iron (III) chloride ($FeCl_3$), selenium, sodium oleate, acrylamide, 2,2′-azobis(2-methylpropionitrile) (AIBN), ammonium acetate (NH_4Ac), 3,4-Methylenedioxy methamphetamine (MDMA), hexadecylamine, tris(hydroxymethyl)aminomethane acetate salt (Trizma® Ac), trioctylphosphine oxide, cerium (iv) sulphate hydrate, trioctylphosphine, oleic acid, sulphur, potassium thiocyanate (KSCN), borax, tetraethyl orthosilicate, 2,2′-azobis(2-methylpropionitrile), zinc chloride, octadecene and sodium acetate (NaAc) were purchased from Merck. 2-(n-Morpholino)ethanesulfonic acid (MES), trisodium citrate, potassium acetate (Kac), diethyl zinc, myristic acid and gold (III) chloride trihydrate ($HAuCl_4.3H_2O$) were purchased from Thermo Fisher.

2.2. Equipment

Ultraviolet/visible (UV/vis) absorption and fluorescence emission measurements were performed using a Varian Cary Eclipse spectrophotometer. The settings used for the fluorescence measurements are Excitation and Emission slit = 10 nm; Scan control = medium; Smoothing = moving average with a factor of 99; Excitation filter = 250–395 nm; Emission filter = 550–1100 nm and PMT detector voltage = high. Transmission electron microscopy (TEM) analysis were carried using a JEOL JEM-1200EX operated at 80 kV. Powder X-ray diffraction (PXRD) analysis was carried out using a Siemens D5000 diffractometer with Cu Kα radiation (λ = 1.54056 nm) and data were obtained in the range of 3–90° using a 0.1° 2θ step size and a 3 s count time per step with a 0.066° slit width. Dynamic light scattering (DLS) was carried out using a Zetasizer Nano ZS series (ZEN3600, Malvern). Energy dispersive X-ray (EDX) analysis was carried out using a JEOL JSM 7400 F field emission scanning electron microscope (SEM) integrated with an Oxford Instruments Inca EDX spectrometer. Fourier transform-infrared (FT-IR) analysis was performed using an Agilent Cary 630 FT-IR spectrometer.

2.3. Synthesis of NH_2-silica-AuZnCeSeS QDs

2.3.1. Preparation of the precursors

Au metal precursor was prepared by first synthesizing citrate-Au nanoparticle (AuNPs). Briefly, hydrophilic citrate-capped AuNPs were synthesized by mixing 1 mL $HAuCl_4.3H_2O$ with 79 mL of ultrapure Milli-Q H_2O and a 20 mL solution containing 4 mL 1% trisodium citrate +0.5 mL 1% tannic acid +15.5 mL ultrapure Milli-Q H_2O was added. The solution was vigorously stirred under heat for ~15 min (min) with the temperature reaching 65°C. The synthesized citrate-capped AuNPs was then converted to hydrophobic hexadecylamine-capped AuNPs via a ligand exchange reaction. The ligand exchange reaction was prepared by dissolving 2 g hexadecylamine in 25 mL toluene and 50 mL of the citrate-AuNPs was added. The solution was stirred for few seconds and kept still until the hydrophilic phase separated from the hydrophobic phase. The hexadecylamine-capped AuNPs was carefully pipetted out from solution and kept in a sealed vial [29].

Selenium precursor was prepared by dissolving 0.12 g selenium in 3 mL of trioctylyphosphine through sonicating the solution under heat to break down the selenium pellets.

Sulphur precursor was prepared by dissolving 0.16 g of sulphur and 0.9 g trioctylyphosphine oxide in 1 mL trioctylyphosphine, 10 mL octadecene and 5 mL oleic acid.

2.3.2. Synthesis of hydrophobic AuZnCeSeS QDs

The synthesis of AuZnCeSeS QDs was carried out using the classic hot-injection organometallic pyrolysis of metal precursors [41,42]. Briefly, 1.2 g diethyl zinc, 1.2 g cerium (IV) sulphate, 1.8 g trioctylyphosphine oxide, 2 mL trioctylyphosphine, 0.6 g hexadecylamine, 0.6 g myristic acid, 25 mL octadecene, 15 mL oleic acid and 3 mL hexadecylamine-capped AuNPs were added into a 3-necked flask, heated and stirred under reflux. When the temperature of the solution reached ~260°C, 3 mL of the selenium precursor and all of the sulphur precursor solution were added. Growth of the hydrophobic AuZnCeSeS QDs proceeded for ~25 min with the solution temperature reaching 270 °C. The reaction was stopped and the hydrophobic AuZnCeSeS QDs were purified using acetone-ethanol, chloroform-acetone-ethanol and acetone.

2.3.3. Preparation of silica-coated AuZnCeSeS QDs

Hydrophobic AuZnCeSeS QDs were first capped with MPA to render the QDs hydrophilic prior to the silica coating. MPA-capped AuZnCeSeS QDs were prepared via a ligand exchange reaction involving the ligand replacement of the hydrophobic capping on the QDs surface with MPA. MPA-KOH-methanolic solution was prepared by dissolving 3 g KOH and 3 mL MPA in 40 mL methanol. Thereafter, the hydrophobic AuZnCeSeS QDs (dissolved in chloroform) was added into the MPA-KOH-methanolic solution and the solution was stirred for few min to aid separation of the organic capping from the QDs surface. The prepared MPA-AuZnCeSeS QDs were purified using acetone. Silica coating on the MPA-AuZnCeSeS QDs was carried out afterward by mixing 37 mg of MPA-AuZnCeSeS QDs with 4 mL 3-aminopropyl)triethoxysilane, 5 mL tetraethyl orthosilicate, 2 mL NH_3·OH and 20 mL methanol. The reaction

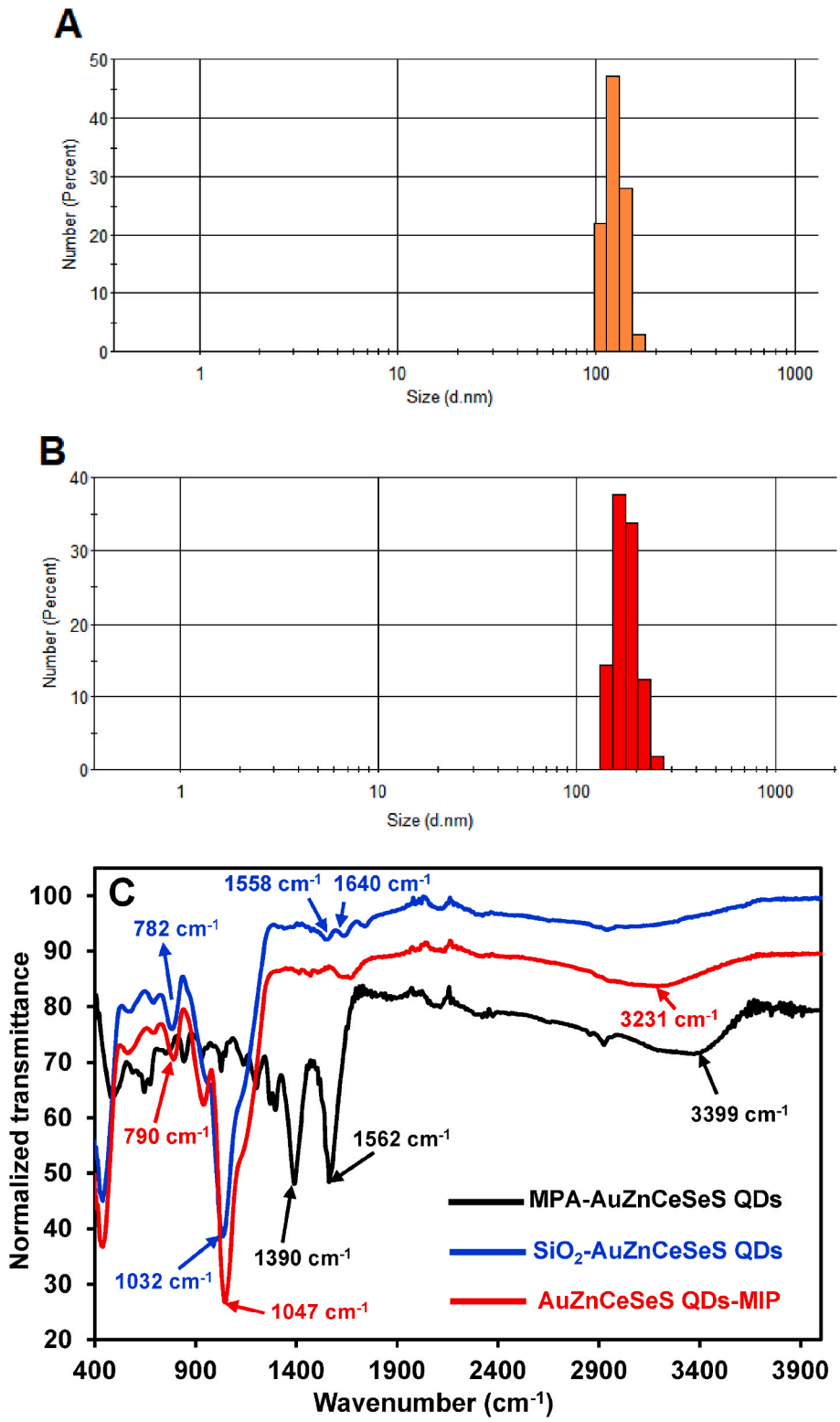

Fig. 3. DLS plots for (A) SiO_2-AuZnCeSeS QDs and the (B) AuZnCeSeS QDs-MIP nanocomposite. (C) FT-IR spectra for MPA-AuZnCeSeS QDs, SiO_2-AuZnCeSeS QDs and the AuZnCeSeS QDs-MIP nanocomposite.

mixture was stirred for 15 min at ambient condition and purified with acetone, ethanol, chloroform acetone and ethanol.

2.4. Preparation of AuZnCeSeS QDs-MIP nanocomposite

The preparation of the AuZnCeSeS QDs-MIP core/shell nanocomposite was carried out via a free radical polymerization reaction as reported in the literature but with slight modifications [29,43]. Pre-polymerization of the polymer in the presence of the METH template was the first step in the imprinting process and was carried out by mixing 150 mg NH_2-silica-AuZnCeSeS QDs with 100 mg acrylamide, 2 mL EGDMA, 100 mg METH and 100 mL acetonitrile. The reaction

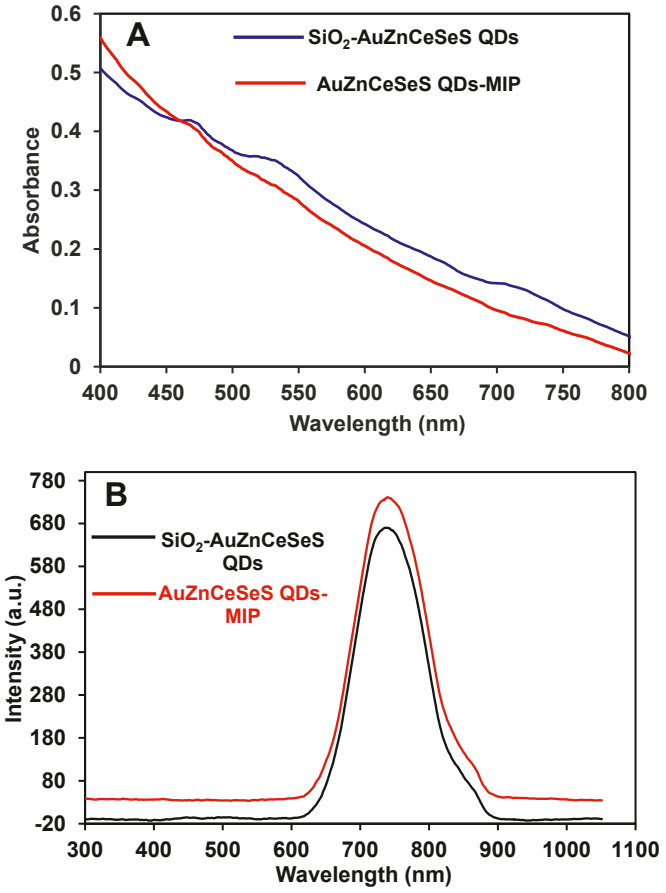

Fig. 4. (A) UV/vis absorption and (B) fluorescence emission spectra of the SiO_2-AuZnCeSeS QDs and the AuZnCeSeS QDs-MIP nanocomposite.

mixture was sonicated and pre-polymerized for ~22 h in the dark. Thereafter, 200 mg AIBN was added into the pre-polymerized solution and the solution was sonicated and kept in a water bath for ~24 h at 60°C, allowing the polymerization reaction to reach completion. The METH template was removed using ethanol:acetic acid, ethanol and acetone via sonication.

2.5. Fluorescence assay for METH detection

The buffer solution used for METH detection was prepared by mixing 5 g each of KSCN, NH_4Ac, borax (B) and 2 g each of MES and Trisma Ac in 250 mL of ultrapure Milli-Q H_2O. The fluorescence assay was carried out by mixing 200 μL of the AuZnCeSeS QDs-MIP nanocomposite in PBS pH 7.4 buffer with 180 μL of METH prepared in KSCN-NH_4Ac-B-MES-Trisma Ac buffer, pH 4 in a quartz cuvette. The fluorescence measurement was undertaken ~15 s after adding the probe solution and the target drug into the cuvette. Measurements were taken in the fluorescence wavelength range from 210 to 1100 nm at an excitation wavelength of 200 nm.

3. Results and discussion

3.1. Fabrication of the AuZnCeSeS QDs-MIP nanocomposite

To fabricate the AuZnCeSeS QDs-MIP nanocomposite, the QDs were synthesized via the organometallic hot-injection pyrolysis of organophosphorus compounds, organic capping agents and metal chalcogenide precursors. It has been well reported in the literature that metal components of groups III-V and II-VII of the periodic table including Cd, Se, Te, Zn, S, In and P, are suitable metal chalcogenides for QDs synthesis [44]. Materials such as AuNPs, carbon, molybdenum, and silicon have generally been used as dopants to finetune the photophysical properties of the QDs [45]. In order to generate a strong plasmonic-exciton (electron and hole) process that could alter the electro-optical properties of QDs and lead to new optical properties, AuNP was used as a dopant for the QDs as reported in this work. Particularly, due to the QDs large absorption cross section and long exciton lifetime, colloidal QD nanocrystals have been widely used as nanofluorophores to develop efficient coupled systems with nanoscale precision and uniquely defined structures [46]. Hence, following up from our recent study on the fabrication of a silica-coated AuZnFeSeS QDs-MIP nanocomposite for levamisole detection [29], we have replaced Fe with Ce in the QDs structure to form a novel fluorescent AuZnCeSeS QDs emitting in the near infra-red region.

Generally, the synthesis of AuZnCeSeS QDs involved the blended use of organophosphorus compounds (trioctylyphosphine and trioctylyphosphine oxide), organic ligands including myristic acid, hexadecylamine and oleic acid, non-coordinating solvent including ODE and the metal precursors. Specifically, the QDs growth was precisely controlled by the organic precursor materials. Once optimum dissolution of diethyl zinc, hexadecylamine-capped AuNPs and cerium (IV) sulphate was achieved in the reaction system with the blended organophosphorus compounds and organic ligands, selenium and sulphur precursors were concurrently added into the growth solution to aid the formation of AuZnCeSeS quintenary alloyed QDs. Since excess amount of diethyl zinc and cerium (IV) sulphate were used, we believe it aided the effective growth of the QDs when the selenium and sulphur precursors were added into the system. Hence, we generally expect three reaction conditions to have occurred according to Equations (1)–(3):

$$\text{Au-CeZn (M)}_x + \text{Se precursor} \rightarrow \text{(Au-CeZnSe)(N)}_y\text{(O)}_z\ k_1 \quad (1)$$

$$\text{Au-CeZn (M)}_x + \text{S precursor} \rightarrow \text{(Au-CeZnS)(N)}_y\text{(O)}_z\ k_2 \quad (2)$$

$$\text{G(Au-CeZnSe)(N)}_y\text{(O)}_z + \text{H(Au-CeZnS)(N)}_y\text{(O)}_z \rightarrow \text{Au-Ce}_a\text{Zn}_b\text{Se}_c\text{S}_d)\ \text{(N)}_y\text{(O)}_z \quad (3)$$

M denotes the solvent and/or surfactants, O denotes the surfactants, selenium precursor and sulphur precursor, while k_1 and k_2 denotes the rate constants of the reaction solution 1 and 2. Reaction 1 involved the interaction of Au-CeZn with the selenium precursor to form Au-CeZnSe nuclei while reaction 2 involved the interaction between Au-CeZn and the sulphur precursor to form Au-CeZnS nuclei. This interactive process led to the formation of rate constants k_1 and k_2. The nanocrystal growth to form $\text{Au-Ce}_a\text{Zn}_b\text{Se}_c\text{S}_{d,}$ is illustrated by reaction 3. It is important to emphasize that reactions 1–3 depends strongly on the type of precursor and solvent, concentration of precursor, reaction time and reaction temperature. The precursors used in the QDs synthesis can be classified as coordinating, weakly coordinating and non-coordinating. Octadecene is a non-coordinating solvent while the other surfactants and organic ligands can be classified as coordinating ligands with differing donation power. Trioctylyphosphine oxide, oleic acid and myristic acid (via the oxygen atom), the sulphur precursor (via the sulphur atom) and trioctylyphosphine (via the phosphine atom) are classified as metal-site coordinating ligands [47].

The hydrophobic QDs were functionalized with MPA via a ligand exchange reaction to render the QDs hydrophilic, stable, biocompatible and dispersible in aqueous solution. To make the QDs compact and suitable for robust MIP shell layering, silica was coated around the MPA-capped QDs surface. The MIP coating process on the QDs surface involved a free radical polymerization core/shell reaction where the QDs functioned as the core and the MIP as the shell. Acrylamide being used as the functional monomer and EGDMA being used as the cross-linker were prepolymerized with the QDs and METH template. It is expected that non-covalent hydrogen bonding should be the predominant binding interaction for the reaction. To fully complete the polymerization reaction, AIBN, functioning as an initiator, was added into the

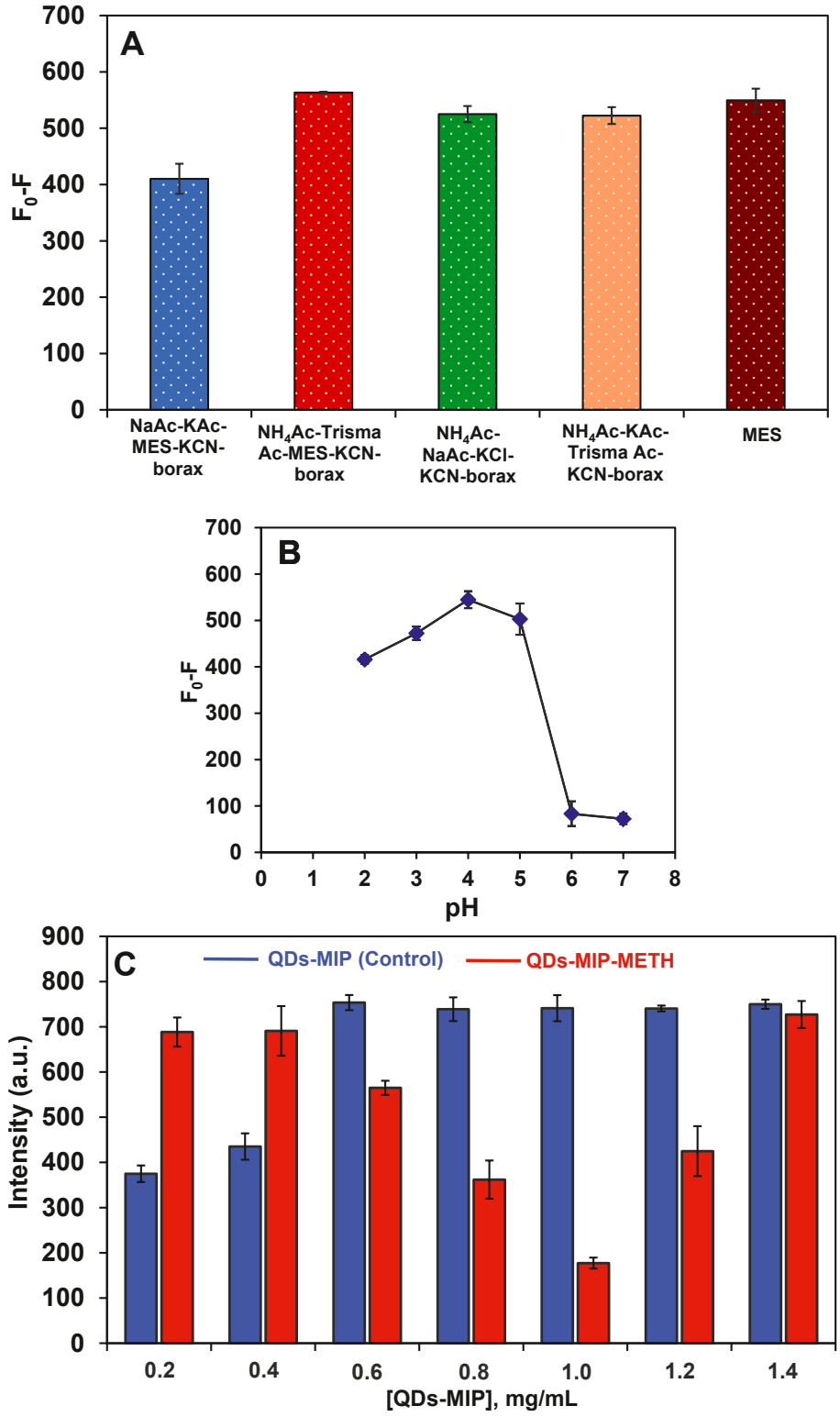

Fig. 5. Fluorescence intensity signal showing the effects of (A) buffer type, (B) pH and (C) QDs-MIP concentration for METH detection using the AuZnCeSeS QDs-MIP nanocomposite probe. F_0 = AuZnCeSeS QDs-MIP solution (no METH) (control); F = AuZnCeSeS QDs-MIP probe solution + METH. [METH] = 50 μM.

prepolymerization reaction to complete the polymerization reaction. Fig. S1 shows the molecular structure of acrylamide, EGDMA, AIBN, METH and the possible mode of hydrogen bonding interaction.

3.2. TEM analysis

TEM analysis of MPA-capped AuZnCeSeS QDs, SiO_2-AuZnCeSeS QDs and the AuZnCeSeS QDs-MIP nanocomposite was carried out to probe the QDs internal structure and to unravel how the morphology of the QDs was affected by the different surface modification processes. For

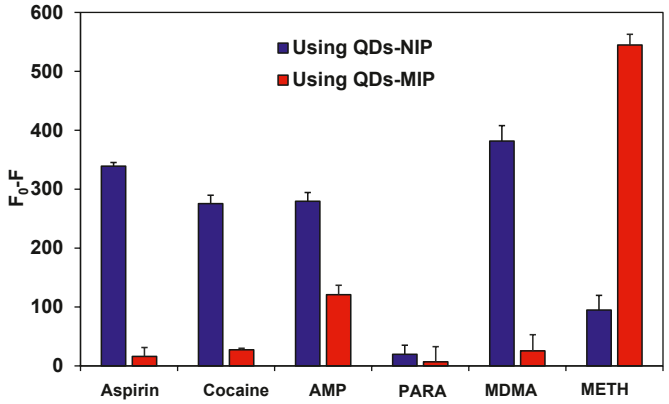

Fig. 6. Fluorescence intensity signal for METH detection in comparison to other non-targeted drugs using the QDs-NIP and QDs-MIP nanocomposite probe. [METH] = 50 μM. METH = methamphetamine; AMP = amphetamine hydrochloride; PARA = paracetamol and MDMA = 3,4-methylenedioxy methamphetamine.

MPA-capped AuZnCeSeS QDs, the TEM image shown in Fig. 1A revealed a mixture of quasi-spherical shaped particles and irregularly shaped particles that were relatively stacked together. Based on this observation, it is justifiable to say that the nucleation and growth of the QDs was heterogenous in nature. The estimated average particle size of the QDs was ~19 nm. Silica coating on the QDs surface revealed several irregularly shaped lumps of particles with characterized rough edges spread across the TEM monograph (Fig. 1B). The observed morphological feature showed clearly that silica coating on the QDs surface altered the QDs particle geometry. For the AuZnCeSeS QDs-MIP nanocomposite (Fig. 1C), the TEM monograph revealed a highly dense particle distribution with the particles stacked together in lumps of irregular shapes.

3.3. PXRD analysis

In order to further understand the effect of the surface modification processes on the QDs surface, PXRD pattern of MPA-AuZnCeSeS QDs, SiO_2-AuZnCeSeS QDs and the AuZnCeSeS QDs-MIP nanocomposite were analysed. As shown in Fig. 2A, the XRD pattern of MPA-AuZnCeSeS QDs was characterized by three prominent peaks assigned to planes {111}, {220} and {311} at 2 theta values of 28 °, 47 ° and 55 ° respectively. Judging by the nature of the diffraction pattern, it is reasonable to define MPA-AuZnCeSeS QDs diffraction pattern as resembling that of a zinc blende crystal structure which is a popular diffraction pattern for group II – VI and III – V QDs class. The diffraction pattern of MPA-AuZnCeSeS QDs also corresponds to the QDs pattern with assigned "JCPDS Card Number 19–0191" [48] as documented by the International Centre for Diffraction Data (ICDD). Following the subsequent surface modifications on the QDs surface, the diffraction pattern of SiO_2-AuZnCeSeS QDs and AuZnCeSeS QDs-MIP were each characterized by a strong single peak around 24 ° (Fig. 2B). The transformational change in the QDs

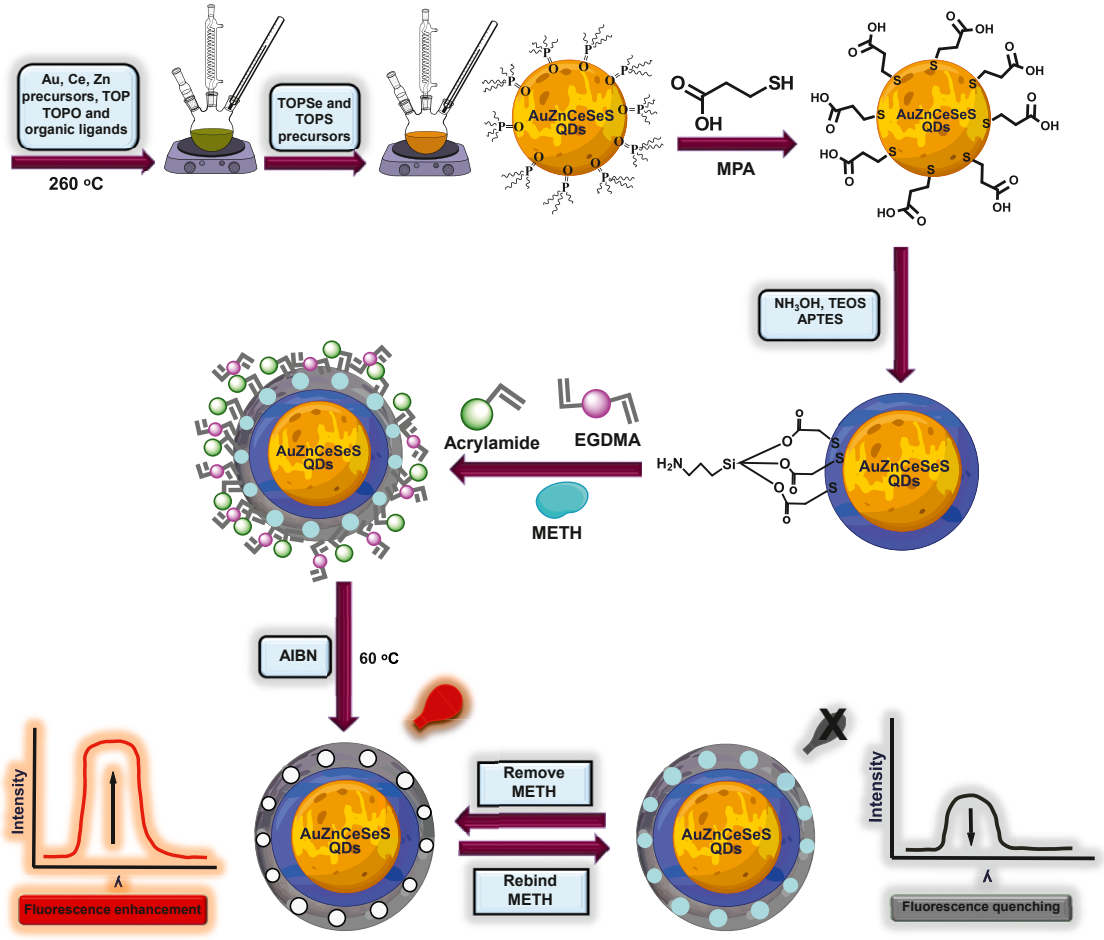

Scheme 1. Schematic representation of the organometallic synthesis of AuZnCeSeS QDs, ligand exchange surface reaction with MPA to form MPA-AuZnCeSeS QDs and surface coating with SiO_2 to form NH_2-SiO_2-AuZnFeSeS QDs; formation of a pre-polymerization complex on the QDs surface in the presence of the monomer, crosslinker and METH template; formation of the MIP shell layer on the QDs core surface in the presence of the initiator and removal and rebinding of METH on the AuZnCeSeS QDs-MIP surface. Rebinding of METH triggered fluorescence turn OFF transduction changes for its detection.

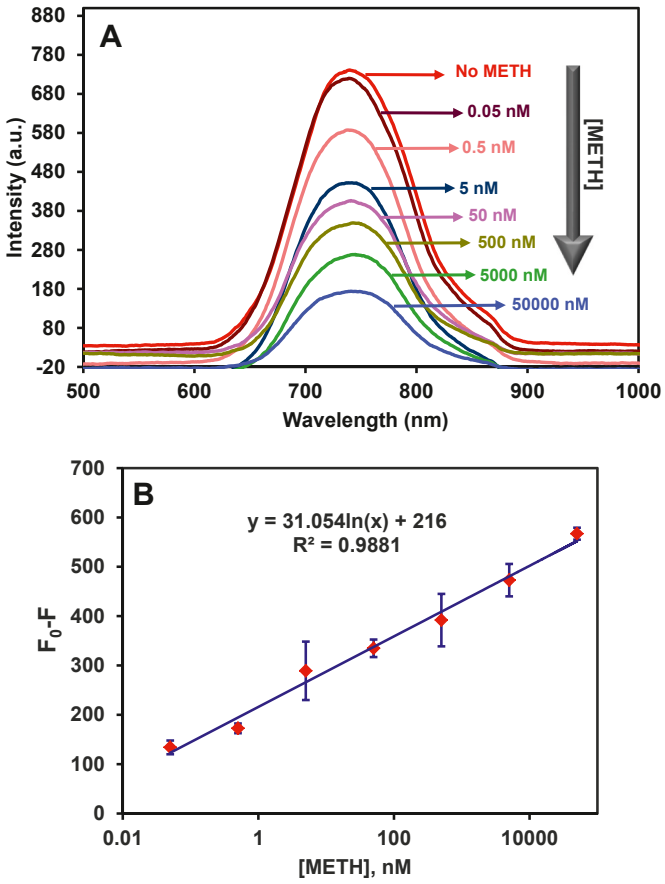

Fig. 7. (A) Fluorescence emission spectra for quantitative METH detection using the AuZnCeSeS QDs-MIP probe. (B) Corresponding calibration signal plot for quantitative METH detection. F_0 = AuZnCeSeS QDs-MIP solution (No METH) (control); F = AuZnCeSeS QDs-MIP probe solution + METH.

Table 1
Analytical parameters of the AuZnCeSeS QDs-MIP nanoprobe for METH detection in comparison to other published probes.

Probe	Method	Concentration detection range	LOD (ng/mL)	Ref.
Graphene QDs-MIP	Fluorescence	5–50 μM	1.7	[40]
$[Ru(bpy)_3]^{2+}$/Nafion	Electrochemiluminescence	0.1 μM - 0.5 mM	13.85	[55]
N,N′-(1,4-phenylene)-dibenzenesulfonamide	Electrochemistry	–	400	[56]
Nanostructure-based [a]SERS chips	SERS	50 μg/mL - 5.0 pg/mL	50	[57]
Aptamer-polycarbonate AuNPs	FT-IR	0.5–10 μM	2	[58]
	Electrochemistry		5	
AgNPs-[a]PDMS substrate	SERS	10^{-4} – 10^{-7} M	185.7	[59]
$[Ru(bpy)_3]^{2+}$ Nafion composite films	Electrochemiluminescence	1 mM - 50 pM	~9.3	[60]
BSA–METH-antibody	Fiber optic particle plasmon resonance	1–1000 ng/mL	0.16	[61]
Aggregation-induced emission- luminogen of tetrakis(4-(pyridin-4-yl) phenyl) ethene- cucurbit [7]uril	Fluorescence	–	79.8	[62]
Nanodiamond-derived carbon nano-onions	Eletrochemistry	0.099–7.48 μM and 7.48–59.88 μM	5.6	[63]
CdS QDs	Fluorescence	6.7–400 μg/L	1.8	[10]
	Chemiluminescence	0.25–125 μg/L	0.086	
Carbon QDs-MIP	Fluorescence	5.0–250 μM	287.1	[64]
MIP-MWCNTs	Eletrochemistry	1.0×10^{-8} – 1.0×10^{-4} M	~0.2	[65]
AuZnCeSeS QDs-MIP	Fluorescence	0.05–50,000 nM	0.0036	**This work**

[a] SERS = Surface enhanced Raman spectrsocopy; PDMS = Polydimethylsiloxane; BSA = Bovine serum albumin; MWCNTs = Multi-walled carbon nanotubes.

diffraction pattern following the SiO_2 and MIP coating, proves to show that surface chemistry played a crucial role in the structural properties of the QDs as it relates to its crystallinity. Judging from similarities in the diffraction pattern of SiO_2-AuZnCeSeS QDs and AuZnCeSeS QDs-MIP with reported XRD pattern for SiO_2 coated QDs [49] and amorphous silica [50], it is reasonable to conclude that the diffraction pattern of SiO_2-AuZnCeSeS QDs and AuZnCeSeS QDs-MIP arises from the strong silica coating on the QDs surface.

3.4. EDX analysis

EDX was used to qualitatively and quantitatively probe the elemental

Table 2
Analytical parameters for METH detection in urine using the AuZnCeSeS QDs-MIP fluorescence probe.

Matrix	METH added, nM	Found (nM)	Recovery (%)	RSD (%, n = 3)
Urine	0.05	~0.06	110.4	~2.4
	0.5	0.50	100.4	8.6
	50	~50	99.8	7.9

composition of the metal chalcogenides that made up the QDs structure. As shown in Fig. S2, peaks corresponding to the QDs metal components of Au, Zn, Ce, Se and S were detected while C and O, which are functional moieties embedded in the MPA ligand structure, were also qualitatively detected. The percentage elemental composition obtained are Au (0.7%), Zn (45.2%), Ce (1.7%), Se (9.6%), S (~17.8%), C (14.8%) and O (6.4%). From the results, it showed clearly that the QDs was highly rich in Zn with the % elemental composition following the order Zn > S > C > Se > O > Ce > Au. More importantly, the result confirmed the successful fabrication of the QDs used in the construction of the QDs-MIP nanocomposite probe.

3.5. DLS analysis

DLS was used to determine the hydrodynamic particle size of the QDs and that of the QDs-MIP nanocomposite. The value obtained was then used to judge the agglomerated state and level of dispersity of the nanomaterials in solution. Generally, when the hydrodynamic size value of colloidal NPs is < 100 nm, the NP is judged to be monodispersed in solution; whereas, when the NPs hydrodynamic size value is > 100 nm, the NP is judged to be polydisperse in solution [51]. It is however important to note that several aggregated induced NPs have been used to develop sensor detector systems [52]. Therefore, high hydrodynamic size value > 100 nm should necessarily not be used to judge the NP physicochemical properties as other factors such as the nanomaterials composition, surface modification and structure, may influence the nanomaterials hydrodynamic size value. Another important advantage of DLS is that it can be used as a tool in surface chemistry to gather information on binding events. Fig. 3A and B shows the DLS histogram plots for SiO_2-AuZnCeSeS QDs and the AuZnCeSeS QDs-MIP nanocomposite. From the plots, the histogram size value for SiO_2-AuZnCeSeS QDs was 125.4 nm and that of the AuZnCeSeS QDs-MIP nanocomposite was 178.2. Based on this result, it is reasonable to conclude that both the QDs and the QDs-MIP were polydispersed in solution. We believe the polydispersity of the nanomaterials arises from the bulky SiO_2 coating on the QDs surface and the MIP coating. The increase in hydrodynamic size value of the QDs-MIP relative to the QDs can also be used to confirm the MIP coating on the QDs surface as the entities on the QDs surface became bulkier.

3.6. FT-IR analysis

FT-IR analysis was used to understand the surface properties of the nanomaterials as it relates to the surface modifications on the QDs. Fig. 3C shows the FT-IR spectra of MPA-AuZnCeSeS QDs, SiO_2-AuZnCeSeS QDs and the AuZnCeSeS QDs-MIP nanocomposite. For MPA-AuZnCeSeS QDs, the bands at 1390 cm^{-1} and 1562 cm^{-1} are attributed to the symmetric and asymmetric stretching band for COO- while the band at 3399 cm^{-1} is ascribed to the O-H stretching vibration. The observed feature confirms the functionalization of MPA on the QDs surface. For SiO_2-AuZnCeSeS QDs, the peaks at 782 cm^{-1} and 1031 cm^{-1} can be ascribed to the Si-O and Si-O-Si stretching vibration while the peaks at 1558 cm^{-1} and 1640 cm^{-1} can be attributed to the N-H bending and C=O stretching vibration. The observed feature definitely confirms the coating of SiO_2 on the QDs surface. For the AuZnCeSeS QDs-MIP nanocomposite, the Si-O (790 cm^{-1}) and Si-O-Si (1047 cm^{-1}) bands were shifted to higher wavenumber in comparison to the SiO_2-AuZnCeSeS QDs. Also, the N-H bending and C=O stretching vibration peaks that were clearly projected in the FT-IR spectrum of the SiO_2-AuZnCeSeS QDs, were not overly projected in the FT-IR spectrum of the QDs-MIP nanocomposite. These changes may be due to the MIP coating process on the QDs surface.

3.7. UV/vis absorption and fluorescence analysis

UV/vis absorption spectra of SiO_2-AuZnCeSeS QDs and the AuZnCeSeS QDs-MIP nanocomposite are shown in Fig. 4A. From the UV/vis absorption feature, both SiO_2-AuZnCeSeS QDs and the AuZnCeSeS QDs-MIP nanocomposite absorption spectra were characterized by broad absorption with no notable excitonic absorption peak. Generally, it is believed that the absorption broadening may arise from the heterogenous nature of the QDs growth. With respect to the QDs absorption broadening, the QDs growth process can be classified according to three different phenomena: (i) coherent epitaxial with significant distortion and strain effect, (ii) incoherent epitaxial with dislocation and strain and (iii) highly disordered [53]. Analysing these three growth possibilities, one can directly rule out highly disordered growth process since the crystallinity of the QDs was confirmed with PXRD. The other two growth process are difficult to analyse because the TEM image of the QDs did not display any vivid picture of lattice plane extension that interprets the QDs growth as coherently epitaxial in nature. We believe as the QDs grew with time, the formation of dislocation and low-angle grain boundaries could have triggered the QDs to grow incoherently and induce some degree of defect state on the QDs surface leading to the absorption broadening [54].

Fluorescence emission spectra of the SiO_2-AuZnCeSeS QDs and the AuZnCeSeS QDs-MIP nanocomposite are shown in Fig. 4B. From the displayed data, SiO_2-AuZnCeSeS QDs fluorescence was characterized by a relatively narrow emission spectrum at a wavelength maximum of 744 nm. This implies the QDs emitted at the near infrared region. This may have been induced by the QDs synthetic process which takes into consideration the influence of the metal precursors and the synthetic parameters such as the concentration of the precursors, precursor ratio, synthetic temperature and reaction time. For the AuZnCeSeS QDs-MIP nanocomposite, no significant peak shift and tailing was observed, suggesting that the imprinting process did not distort the QDs fluorescence geometry. Hence, confirming the QDs fluorescence stability during the imprinting process. The main observation in the fluorescence emission spectrum of the AuZnCeSeS QDs-MIP nanocomposite, is the enhancement in fluorescence emission relative to the SiO_2-AuZnCeSeS QDs. This implies that the imprinting effect passivated the surface of the QDs by inducing radiative exciton recombination.

3.8. Optimization

Optimization reaction steps including the effects of buffer, pH and the QDs-MIP concentration were investigated. Fig. 5A shows the effect of buffer type on the fluorescence intensity signal for METH detection using the AuZnCeSeS QDs-MIP nanoprobe. METH concentration of 50 μM was prepared in five different buffers, namely: NaAc-KAc-MES-KCN-borax, NH_4Ac-Trisma Ac-MES-KCN-borax, NH_4Ac-NaAc-KCl-KCN-borax, NH_4Ac-KAc-Trisma Ac-KCN-borax and MES. The result showed that the sensitivity of the AuZnCeSeS QDs-MIP nanoprobe for METH detection in the tested buffer followed the order: NH_4Ac-Trisma Ac-MES-KCN-borax > MES > NH_4Ac-NaAc-KCl-KCN-borax > NH_4Ac-KAc-Trisma Ac-KCN-borax > NaAc-KAc-MES-KCN-borax. From the obtained result, NH_4Ac-Trisma Ac-MES-KCN-borax buffer was chosen as the choice buffer for METH fluorescence detection.

The effect of pH on the fluorescence detection of METH using the AuZnCeSeS QDs-MIP nanocomposite probe was also investigated. METH was prepared in NH_4Ac-Trisma Ac-MES-KCN-borax buffer, pH 2–7 and the resulting fluorescence intensity signal is shown in Fig. 5B. From the obtained data, the fluorescence intensity signal increased steadily from

pH 2, reaching a maximum intensity signal at pH 4 and then declined afterward from pH 5 to 7. Based on this observation, pH 4 was chosen as the choice pH for METH detection.

The effect of AuZnCeSeS QDs-MIP concentration tested from 0.2 to 1.4 mg/mL on the fluorescence intensity signal for METH detection was also investigated. Fig. 5C shows the effect of varying concentrations of the QDs-MIP nanoprobe on the fluorescence intensity signal for METH. At lower concentration of the QDs-MIP, specifically at 0.2 and 0.4 mg/mL, the fluorescence intensity signal for METH detection was enhanced relative to the control. Conversely, from 0.6 mg/mL up until the maximum tested concentration of 1.4 mg/mL, the fluorescence intensity signal of the AuZnCeSeS QDs-MIP nanoprobe was quenched by the targeted METH analyte. Generally, as the probe concentration increased in the system from 0.6 mg/mL upward, the fluorescence quenching effect induced by METH reached maximum intensity at 1 mg/mL and declined afterward up until 1.4 mg/mL. Judging from the obtained result, 1 mg/mL was chosen as the choice QDs-MIP probe concentration for METH fluorescence detection.

3.9. Selectivity of the nanosensor

The efficacy of the AuZnCeSeS QDs-MIP nanocomposite probe to fluorescently detect METH was investigated and compared to the data obtained using the AuZnCeSeS QDs-NIP nanocomposite. Fig. 6 shows the fluorescence intensity signal obtained for METH in comparison to the intensity response obtained for aspirin, cocaine, AMP, PARA and MDMA using the QDs-MIP and QDs-NIP nanocomposite probes. From the result, the fluorescence intensity signal obtained for METH using the QDs-MIP probe was far superior to the response obtained for the non-targeted drugs. On the other hand, the fluorescence response obtained for the tested drugs using the QDs-NIP probe did not generate any form of selectivity. Hence, it is noteworthy to state that METH was able to selectively rebind into the created cavities in the MIP shell around the QDs core surface and this triggered the bound QDs to report the generated fluorescence intensity signal in a selective fashion for METH.

3.10. Reaction mechanism

The mechanistic reaction process for METH detection using the QDs-MIP nanocomposite probe can be explained in terms of METH template imprinting, METH template removal, METH template re-binding and fluorescence signal transduction. As shown in Scheme 1, AuZnCeSeS QDs were synthesized in the presence of organic ligands and metal precursors. This allowed the nucleation and subsequent growth of the QDs and the capping of its surface with organic ligands. A ligand exchange reaction was then performed to remove the organic capping agents and cap the QDs surface with water-soluble MPA thiol ligand. This was done to render the QDs biocompatible, hydrophilic and stable in the aqueous phase. Silica, functioning as a rigid coating layer, was coated around the QDs surface to make the QDs compact and to aid robustness of the MIP process which was to follow afterward. During the silica coating process, the functional monomer was APTES, the cross-linker was TEOS and NH_3·OH served as the catalyst. The amino functional moieties of APTES can interact with the functional moieties of acrylamide via non-covalent hydrogen bonding. It is also possible for acrylamide to interact with the METH template in a non-covalent fashion while EGDMA and AIBN served to aid completion of the polymerization imprinting reaction. The removal of METH from the MIP shell during purification, allowed cavities of specific size and shape to be created. Due to the MIP shell also acting as a passivating layer on the QDs surface, the fluorescence of the bound QDs was enhanced relative to the unbound QDs. The interaction of METH with the QDs-MIP nanoprobe ensured a rebinding process was triggered in which the targeted METH drug was able to precisely rebind into the created cavities on the MIP shell. The QDs-MIP-METH rebinding process allowed the bound QDs to transduce the fluorescence signal via a non-radiative recombination (fluorescence quenching) process in a selective and highly sensitive fashion. The overall reaction can be termed as a fluorescence ON-OFF process.

3.11. Quantitative METH detection

Quantitative detection of METH was carried out using the QDs-MIP nanocomposite probe. Fig. 7A shows the quantitative spectral response for METH detection using the QDs-MIP probe in the concentration range of 0.05–50,000 nM. As increasing concentration of METH was added into the nanoprobe system, steady decrease in the fluorescence emission intensity was observed. The observed result proved to show that the QDs-MIP nanoprobe can quantitatively detect METH over a wide concentration range. The corresponding calibration plot shown in Fig. 7B was used to assess the sensitivity of the nanoprobe by determining the limit of detection (LOD). The LOD was calculated using the formula LOD $= 3\ \delta/K$, where δ = standard deviation of blank measurements (n = 10) and K = slope of the linear calibration plot. The calculated LOD for METH detection using the QDs-MIP nanocomposite probe was ~0.02 nM (0.0036 ng/mL). In order to properly judge the sensitivity of our developed probe, we compared the obtained analytical parameters with data from published probes as shown in Table 1. From the comparative results shown in Table 1, it demonstrates clearly that the LOD obtained for METH using the developed AuZnCeSeS QDs-MIP nanoprobe was much lower than published probes, making our detection system the most sensitive ever reported for METH detection.

3.12. Detection in urine

The efficacy of the AuZnCeSeS QDs-MIP nanoprobe to detect METH in urine was investigated. Urine sample was collected according to ethical procedure and used without pre-treatment. METH concentrations of 0.05, 0.5 and 50 nM were spiked in urine sample and analysed using the AuZnCeSeS QDs-MIP nanoprobe. Table 2 shows the obtained analytic merits for METH in urine sample. The results clearly showed that METH can be detected in urine using the AuZnCeSeS QDs-MIP nanoprobe as the recovery efficiency ranged from 99.8 to 110.4%.

4. Conclusions

The development of a novel detection system for METH has been accomplished using a fluorescent AuZnCeSeS QDs-MIP nanocomposite probe. AuZnCeSeS QDs were synthesized and encapsulated in a silica network and characterized using complimentary analytical techniques. Via a free radical polymerization reaction, the QDs surface was coated with a MIP shell of which METH was used as the template. The QDs-MIP nanocomposite purification led to the creation of cavities of specific size and shape that fits the METH structure. METH was selectively detected at ultralow concentration with a detection limit that was far lower than published probes. Detection of METH in urine was successfully achieved using the developed AuZnCeSeS QDs-MIP nanocomposite probe.

CRediT authorship contribution statement

Oluwasesan Adegoke: Writing – review & editing, Writing – original draft, Project administration, Methodology, Investigation, Formal analysis, Data curation, Conceptualization. **M. Laura Nsuamani:** Writing – review & editing, Formal analysis, Data curation. **Niamh Nic Daeid:** Writing – review & editing, Project administration, Funding acquisition.

Declaration of competing interest

The authors declare that they have no known competing financial interests or personal relationships that could have appeared to influence the work reported in this paper.

Data availability

Data will be made available on request.

Acknowledgements

Authors gratefully acknowledge the financial support from Leverhulme Trust (RC-2015-011) for funding this work. OA sincerely appreciates the support received from the School of Science and Engineering, University of Dundee.

Appendix A. Supplementary data

Supplementary data to this article can be found online at https://doi.org/10.1016/j.mssp.2023.107387.

References

[1] B.K. Logan, Amphetamines: an update on forensic issues, J. Anal. Toxicol. 25 (2001) 400–404.
[2] F. Garcia-Bournissen, B. Rokach, T. Karaskov, G. Koren, Methamphetamine detection in maternal and neonatal hair: implications for fetal safety, Arch. Dis. Child. Fetal Neonatal Ed. 92 (2007) 351–355.
[3] B.K. Logan, Methamphetamine—effects on human performance and behavior, Forensic Sci. Rev. 14 (2002) 133–151.
[4] European Drug Report, Available online from: https://www.emcdda.europa.eu/publications/edr/trends-developments/2021_en. (Accessed 26 May 2022).
[5] World Drug Report 2020, United Nations, World Drug Report 2020. (n.d.), https://wdr.unodc.org/wdr2020/en/index.html. (Accessed 23 May 2022).
[6] T. Zhang, X. Chen, R. Yang, Y. Xu, Detection of methamphetamine and its main metabolite in fingermarks by liquid chromatography–mass spectrometry, Forensic Sci. Int. 248 (2015) 10–14.
[7] H. Inoue, K. Kuwayama, Y.T. Iwata, T. Kanamori, K. Tsujikawa, H. Muyaguchi, Simple and simultaneous detection of methamphetamine and dimethyl sulfone in crystalline methamphetamine seizures by fast chromatography, Forensic Toxicol. 26 (2008) 19–22.
[8] J. Welter, P. Kavanagh, M.R. Meyer, H.H. Mauerer, Benzofuran analogues of amphetamine and methamphetamine: studies on the metabolism and toxicological analysis of 5-APB and 5-MAPB in urine and plasma using GC–MS and LC–(HR)-MSn techniques, Anal. Bioanal. Chem. 407 (2015) 1371–1388.
[9] X. Chen, Analysis of methamphetamine in human urine using ionic liquid dispersive liquid-phase microextraction combined with HPLC, Chromatographia 78 (2015) 515–520.
[10] J. Hassanzadeh, A. Khataee, R. Lofti, Sensitive fluorescence and chemiluminescence procedures for methamphetamine detection based on CdS quantum dots, Microchem. J. 132 (2017) 371–377.
[11] M. Rezazadeh, Y. Yamini, S. Seidi, Application of a new nanocarbonaceous sorbent in electromembrane surrounded solid phase microextraction for analysis of amphetamine and methamphetamine in human urine and whole blood, J. Chromatogr. A 1396 (2015) 1–6.
[12] O. Adegoke, S. Zolotovskaya, A. Abdolvand, N. Nic Daeid, Biomimetic graphene oxide-cationic multi-shaped gold nanoparticle-hemin hybrid nanozyme: tuning enhanced catalytic activity for the rapid colorimetric apta-biosensing of amphetamine-type stimulants, Talanta 216 (2020), 120990.
[13] Y. Mohsen, N. Gharbi, A. Lenouvel, C. Guignard, Detection of Δ9-tetrahydrocannabinol, methamphetamine and amphetamine in air at low ppb level using a field asymmetric ion mobility spectrometry microchip sensor, Procedia Eng. 87 (2014) 536–539.
[14] J. Mao, Y. Kang, D. Yu, J. Zhou, Surface-enhanced Raman spectroscopy integrated with aligner mediated cleavage strategy for ultrasensitive and selective detection of methamphetamine, Anal. Chim. Acta 1146 (2021) 124–130.
[15] M. Alijanianzadeh, F. Qadami, A. Molaeirad, Detection of methamphetamine using aptamer-based biosensor chip and cyclic voltammetry technique, J. Indian Chem. Soc. 98 (2021), 100189.
[16] T.-C. Chang, C.-Y. Chiang, M.-H. Lin, I.-K. Chen, L.-K. Chau, D.-S. Hsu, S.-S. Shieh, C.-J. Kuo, S.-C. Wang, Y.-F. Chen, Fiber optic particle plasmon resonance immunosensor for rapid and sensitive detection of methamphetamine based on competitive inhibition, Microchem. J. 157 (2020), 105026.
[17] D. Wen, Y.Y. Fu, L.Q. Shi, C. He, L. Dong, D.F. Zhu, Q.G. He, H.M. Cao, J.G. Cheng, Fine structural tuning of fluorescent copolymer sensors for methamphetamine vapor detection, Sensor. Actuator. B Chem. 168 (2012) 283–288.
[18] J.G. Bramness, M.J. Reid, K.F. Solvik, V. Vindenes, Recent trends in the availability and use of amphetamine and methamphetamine in Norway, Forensic Sci. Int. 246 (2015) 92–97.
[19] R.-R. Zhang, X.-J. Li, A.-L. Sun, S.-Q. Song, X.-Z. Shi, A highly selective fluorescence nanosensor based on the dual-function molecularly imprinted layer coated quantum dots for the sensitive detection of diethylstilbestrol/cypermethrin in fish and seawater, Food Control 132 (2022), 108438.
[20] O. Adegoke, E.Y. Park, Bright luminescent optically engineered core/alloyed shell quantum dots: an ultrasensitive signal transducer for dengue virus RNA via localized surface plasmon resonance-induced hairpin hybridization, J. Mater. Chem. B 5 (2017) 3047–3058.
[21] O. Adegoke, M.-W. Seo, T. Kato, S. Kawahito, E.Y. Park, An ultrasensitive SiO2-encapsulated alloyed CdZnSeS quantum dot-molecular beacon nanobiosensor for norovirus, Biosens. Bioelectron. 86 (2016) 135–142.
[22] L. Liu, H. Chu, J. Yang, Y. Sun, P. Ma, D. Song, Construction of a magnetic-fluorescent-plasmonic nanosensor for the determination of MMP-2 activity based on SERS-fluorescence dual-mode signals, Biosens. Bioelectron. 212 (2022), 114389.
[23] L. Jia, Z. Xu, L. Zhang, Y. Li, T. Zhao, J. Xu, The fabrication of water-stable perovskite-europium hybrid polychromatic fluorescence nanosensor for fast visual sensing of tetracycline, Appl. Surf. Sci. 592 (2022), 153170.
[24] P. Pooja, Chowdhury, Functionalized CdTe fluorescence nanosensor for the sensitive detection of water borne environmentally hazardous metal ions, Opt. Mater. 111 (2021), 110584.
[25] S. Fan, X. Li, F. Ma, M. Yang, J. Su, X. Chen, Sulfur quantum dot based fluorescence assay for lactate dehydrogenase activity detection, J. Photochem. Photobiol. Chem. 430 (2022), 113989.
[26] J. Qiu, L. Na, Y. Li, W. Bai, J. Zhang, L. Jin, N,S-GQDs mixed with CdTe quantum dots for ratiometric fluorescence visual detection and quantitative analysis of malachite green in fish, Food Chem. 390 (2022), 133156.
[27] P.K. Namboothiri, S. Govindan, K.V. Rajitha, S. Jasmine, M. Pter, D.B. Niranjan, S. Umakanth, Dengue NS1 antigen detection using photoluminescence of solution phase biotylinated anti-NS1 antibody conjugated ZnO quantum dots, Mater. Chem. Phys. 279 (2022), 125778.
[28] O. Adegoke, M.A. Pereira-Barros, S. Zolotovskaya, A. Abdolvand, N. Nic Daeid, Aptamer-based cocaine assay using a nanohybrid composed of ZnS/Ag2Se quantum dots, graphene oxide and gold nanoparticles as a fluorescent probe, Microchim. Acta 187 (2020) 104.
[29] O. Adegoke, S. Zolotovskaya, A. Abdolvand, N. Nic Daeid, Fabrication of a near-infrared fluorescence-emitting SiO2-AuZnFeSeS quantum dots-molecularly imprinted polymer nanocomposite for the ultrasensitive fluorescence detection of levamisole, Colloids Surf. A Physicochem. Eng. Asp. 646 (2022), 129013.
[30] T. Niizuma, K. Obinata, H. Ikari, A. Kamata, T. Lee, K. Kinoshita, T. Shimizu, False positive of an immunochromatography kit for detection of norovirus in neonatal feces, J. Infect. Chemother. 19 (2013) 171–173.
[31] G. Wulff, A. Sarhan, The use of polymers with enzyme-analogous structures for the resolution of racemates, Angew. Chem. Int. Ed. 11 (1972) 341–344.
[32] L. Wang, L. Wen, L. Zhao, J. Chao, F. Tao, F. Wang, C. Li, Development of fluorescence sensor and test paper based on molecularly imprinted carbon quantum dots for spiked detection of domoic acid in shellfish and lake water, Anal. Chim. Acta 1197 (2022), 339515.
[33] R.-R. Zhang, X.-J. Li, A.-L. Sun, S.-Q. Song, X.-Z. Shi, A highly selective fluorescence nanosensor based on the dual-function molecularly imprinted layer coated quantum dots for the sensitive detection of diethylstilbestrol/cypermethrin in fish and seawater, Food Control 132 (2022), 108438.
[34] X. Kong, R. Gao, X. He, L. Chen, Y. Zhang, Synthesis and characterization of the core–shell magnetic molecularly imprinted polymers (Fe3O4@MIPs) adsorbents for effective extraction and determination of sulfonamides in the poultry feed, J. Chromatogr. A 1245 (2012) 8–16.
[35] X. Zhang, D. An, R. Zhang, Y. Huang, Z. Liu, Preparation of carbon nanotubes and polyhedral oligomeric-reinforced molecularly imprinted polymer composites for drug delivery of gallic acid, Int. J. Pharm. 615 (2022), 121476.
[36] J. Wackerlig, R. Schirhagl, Applications of molecularly imprinted polymer nanoparticles and their advances toward industrial use: a review, Anal. Chem. 88 (2016) 250–261.
[37] M. Yang, C. Wang, E. Liu, X. Hu, H. Hao, J. Fan, A novel ascorbic acid ratiometric fluorescent sensor based on ZnCdS quantum dots embedded molecularly imprinted polymer and silica-coated CdTeS quantum dots, J. Mol. Liq. 337 (2021), 116438.
[38] L. Wu, Z.-Z. Lin, J. Zeng, H.-P. Zhong, X.-M. Chen, Z.-Y. Huang, Detection ofmalachite green in fish based on magnetic fluorescent probe of CdTe QDs/nano-Fe3O4@MIPs, Spectrochim. Acta Mol. Biomol. Spectrosc. 196 (2018) 117–122.
[39] L. Wang, L. Zhao, A novel nanocomposite optosensing sensor based on porous molecularly imprinted polymer and dual emission quantum dots for visual and high selective detection of bovine serum albumin, Colloids Surf. A Physicochem. Eng. Asp. 632 (2022), 12784.
[40] M. Masteri-Farahani, S. Mashhadi-Ramezani, N. Mosleh, Molecularly imprinted polymer containing fluorescent graphene quantum dots as a new fluorescent nanosensor for detection of methamphetamine, Spectrochim. Acta Mol. Biomol. Spectrosc. 229 (2020), 118021.
[41] L. Hu, H. Zhong, Z. He, Toxicity evaluation of cadmium-containing quantum dots: a review of optimizing physicochemical properties to diminish toxicity, Colloids Surf. B Biointerfaces 200 (2021), 111609.
[42] O. Adegoke, E.Y. Park, Nanofabricated optical tuning and epitaxial overgrowth of In2S3 shells on CdSe cores, New J. Chem. 41 (2017) 1303–1312.
[43] J. Bai, L. Chen, Y. Zhu, X. Wang, X. Wu, Y. Fu, A novel luminescence sensor based on porous molecularly imprinted polymer-ZnS quantum dots for selective recognition of paclitaxel, Colloids Surf. A Physicochem. Eng. Asp. 610 (2021), 125696.
[44] Y. Volkov, Quantum dots in nanomedicine: recent trends, advances and unresolved issues, Biochem. Biophys. Res. Commun. 468 (2015) 419–427.
[45] Q. Ma, X. Su, Near-infrared quantum dots: synthesis, functionalization and analytical applications, Analyst 135 (2010) 1867–1877.
[46] Y. Luo, Y. Wang, M. Liu, H. Zhu, O. Chen, S. Zuo, J. Zhao, Colloidal assembly of Au−quantum dot−Au sandwiched nanostructures with strong plasmon−exciton coupling, J. Phys. Chem. Lett. 11 (2020) 2449–2456.

[47] N. Al-Salim, A.G. Yung, R.D. Tilley, A.J. McQuillan, J. Xia, Synthesis of CdSeS nanocrystals in coordinating and noncoordinating solvents: solvent's role in evolution of the optical and structural properties, Chem. Mater. 19 (2007) 5185–5193.
[48] O. Adegoke, C. McKenzie, N. Nic Daeid, Multi-shaped cationic gold nanoparticle-Lcysteine-ZnSeS quantum dots hybrid nanozyme as an intrinsic peroxidase mimic for the rapid colorimetric detection of cocaine, Sensor. Actuator. B Chem. 287 (2019) 416–427.
[49] S. Chen, Y. Li, S. Wu, X. Jiang, H. Yang, X. Su, L. He, L. Zou, X. Ao, S. Liu, Y. Yang, A phosphorescent probe for cephalexin consisting of mesoporous thioglycolic acidmodified Mn:ZnS quantum dots coated with a molecularly imprinted polymer, Microchim. Acta 187 (2020) 40.
[50] E. Rafiee, S. Shahebrahimi, M. Feyzi, M. Shaterzadeh, Optimization of synthesis and characterization of nanosilica produced from rice husk (a common waste material), Int. Nano Lett. 2 (2012) 29.
[51] O. Adegoke, K. Takemura, E.Y. Park, Plasmonic oleylamine-capped gold and silver nanoparticle-assisted synthesis of luminescent alloyed CdZnSeS quantum dots, ACS Omega 3 (2018) 1357–1366.
[52] E. Priyadarshini, N. Pradhan, Gold nanoparticles as efficient sensors in colorimetric detection of toxic metal ions: a review, Sensor. Actuator. B Chem. 238 (2017) 888–902.
[53] C.-T. Cheng, C.-Y. Chen, C.-W. Lai, W.-H. Liu, S.-C. Pu, P.-T. Chou, Y.-H. Chou, H.-T. Chiu, Syntheses and photophysical properties of type-II CdSe/ZnTe/ZnS (core/shell/shell) quantum dots, J. Mater. Chem. 15 (2005) 3409–3414.
[54] O. Adegoke, T. Nyokong, P.B.C. Forbes, Structural and optical properties of alloyed quaternary CdSeTeS core and CdSeTeS/ZnS core–shell quantum dots, J. Alloys Compd. 645 (2015) 443–449.
[55] E. Dokuzparmark, K. Brown, L. Dennany, Electrochemiluminescent screening for methamphetamine metabolites, Analyst 146 (2021) 3336–3345.
[56] C.-A. Barlett, S. Taylor, C. Fernandez, C. Wanklyn, D. Burton, E. Enston, A. Raniczkowska, M. Black, L. Murphy, Disposable screen printed sensor for the electrochemical detection of methamphetamine in undiluted saliva, Chem. Cent. J. 10 (2016) 3.
[57] N. Nuntawong, P. Eiamchai, W. Somrang, S. Denchitcharoen, S. Limwichean, M. Horprathum, V. Pattanasettakul, S. Chaiya, A. Leelapojanaporn, S. Saiseng, P. Pongsethasant, P. Chindaudom, Detection of methamphetamine/amphetamine in human urine basedon surface-enhanced Raman spectroscopy and acidulation treatments, Sensor. Actuator. B Chem. 239 (2017) 139–146.
[58] M. Alijanianzadeh, F. Qadami, A. Molaeirad, Detection of methamphetamine using aptamer-based biosensor chip and cyclic voltammetry technique, J. Indian Chem. Soc. 98 (2021), 100189.
[59] K. Maneejark, N. Sangwaranatee, N. Chamchoi, N. Kulnides, P. Somboonsaksri, S. Limwichean, T. Pogfay, S. Kalasung, P. Eiamchai, V. Patthanasettakul, N. Limsuwan, N. Triamnak, N. Nuntawong, M. Horprathum, Development of cost-effective fabrication process for on-site methamphetamine detection by adsorbable SERS substrate, Opt. Mater. 124 (2022), 111988.
[60] J. McGeehan, L. Dennany, Electrochemiluminescent detection of methamphetamine and amphetamine, Forensic Sci. Int. 264 (2016) 1–6.
[61] T.-C. Chang, C.-Y. Chiang, M.-H. Lin, I.K. Chen, L.-K. Chau, D.-S. Hsu, S.-S. Shieh, C.-J. Kuo, S.-C. Wang, Y.-F. Chen, Fiber optic particle plasmon resonance immunosensor for rapid and sensitive detection of methamphetamine based on competitive inhibition, Microchem. J. 157 (2020), 105026.
[62] X. Du, H. Hao, A. Qin, B.Z. Tang, Highly sensitive chemosensor for detection of methamphetamine by the combination of AIE luminogen and cucurbit[7]uril, Dyes Pigments 180 (2020), 108413.
[63] Z. Khorablou, F. Shahdost-fard, H. Razmi, Nanodiamond-derived carbon nano-onions decorated with silver nanodendrites as an effective sensing platform for methamphetamine detection, Surface. Interfac. 31 (2022), 102061.
[64] S. Mandani, B. Rezaei, A.A. Ensafi, Sensitive imprinted optical sensor based on mesoporous structure and green nanoparticles for the detection of methamphetamine in plasma and urine, Spectrochim. Acta Mol. Biomol. Spectrosc. 231 (2020), 118077.
[65] M. Akhoundian, T. Alizadeh, M.R. Ganjali, P. Norouzi, Ultra-trace detection of methamphetamine in biological samples using FF-square wave voltammetry and nano-sized imprinted polymer/MWCNTs -modified electrode, Talanta 200 (2019) 115–123.